Journal of Engineering Science and Technology
Special Issue on ISSTEC, November (2021) 122 - 130

SYNTHESIS AND PHOTOELECTROCHEMICAL PROPERTY OF CUBIC-SHAPE $La_2Ti_{1-x}V_xO_7$ NANOCRYSTAL

GANI PURWIANDONO[1,*], PUJI LESTARI[2], TAKASHI SUGIURA[3]

[1]Department of Chemistry, Universitas Islam Indonesia, 55584, Indonesia
[2]Department of Environmental Engineering, Universitas Islam Indonesia, 55584, Indonesia
[3]The Graduate School of Natural Science and Technology, Gifu University, Japan
*Corresponding Author: gani_purwiandono@uii.ac.id

Abstract

The vanadium doping in layered $La_2Ti_2O_7$ could effectively increase the photocatalytical properties of $La_2Ti_2O_7$. The purpose of this research is to synthesise and characterize the photoelectrochemical property of cubic-shape $La_2Ti_{1-x}V_xO_7$ nanocrystal. Cubic-shape $La_2Ti_{1-x}V_xO_7$ nanocrystal was synthesized for the first time by a molten salt-based reaction using La_2O_3, TiO_2 and Na_3VO_4. LiCl as a molten salt could increase the homogeneous phase of $La_2Ti_{1-x}V_xO_7$ nanocrystals. Scanning Electron Microscopy (SEM) and Transmission Electron Microscopy (TEM) measurements revealed that $La_2Ti_{1-x}V_xO_7$ nanocrystals' cubic shape was formed with the average dimensions of 300 nm. The bandgap of cubic-shape $La_2Ti_{1-x}V_xO_7$ was estimated to be 2.62 eV. The photoelectrochemical cell fabricated using the $La_2Ti_{1-x}V_xO_7$ particles electrode exhibited a higher photocurrent than $La_2Ti_2O_7$ under UV light irradiation. The synthetic method of cubic-shape $La_2Ti_{1-x}V_xO_7$ nanocrystals might provide new avenues for producing photoenergy conversion materials.

Keywords: Cubic-shape La2Ti1-xVxO7, Molten salt reaction, Photoelectrochemical property.

1. Introduction

Lanthanum titanate ($La_2Ti_2O_7$) has been broadly investigated because of its unique properties, including the ferroelectric [1, 2], photocatalytic [3-5] and dielectric properties [6, 7]. $La_2Ti_2O_7$ has been widely reported to demonstrate good photocatalytic achievement for organic pollutant degradation [3, 4], CO_2 conversion [2] and water splitting reaction [5, 6]. Recently, the performance of $La_2Ti_2O_7$ has been promoted due to its wide band gap [8]. However, the application of $La_2Ti_2O_7$ was mainly limited to the bare $La_2Ti_2O_7$ [9, 10] $La_2Ti_2O_7$ material with the addition of dopants or impurities to increase the activity of $La_2Ti_2O_7$ are still under-studied [11-13].

Scarrozza et al. using density functional theory, predicted that vanadium doping in layered $La_2Ti_2O_7$ could effectively increase the ferroelectric properties even at high temperatures. This is due to vanadium clustering in diffuse and homogeneous chains retaining the polarization and generating substantial ferromagnetic order simultaneously. High concentration doping is feasible with donor ions with varying lengths in different directions for La^{3+} in $La_2Ti_2O_7$ [14]. Li et al. reported the synthesis of $La_2Ti_{1.96}V_{0.04}O_7$-based ceramic by using the solid-state reaction method. The piezoelectric property of $La_2Ti_{1.96}V_{0.04}O_7$-based ceramic increased compare to the $La_2Ti_2O_7$ ceramics. However, none of the above reports has investigated the morphology control of $La_2Ti_{1-x}V_xO_7$ and its photoelectrochemical properties [15].

We have successfully synthesized the homogeneous structure of GaN and InN using the molten salt reaction [16, 17]. The use of molten salt could accelerate the homogeneous structure formation at the nanoscale. In this work, the synthesis of cubic-shape $La_2Ti_{1-x}V_xO_7$ has been demonstrated for the first time using a molten salt reaction. Our procedure for controlling the growth of $La_2Ti_{1-x}V_xO_7$ provides a new approach to create homogeneous nanocrystals. In $La_2Ti_{1-x}V_xO_7$, the dopant V^{5+} cations with smaller ionic radii have substituted the Ti^{4+} and enhanced the distortions of TiO_6 oxygen octahedron from the basic structure $La_2Ti_2O_7$ [15]. We predicted that the formation of cubic-shape $La_2Ti_{1-x}V_xO_7$ could enhance the photoelectrochemical cells' donor density compared to $La_2Ti_2O_7$.

2. Experimental Method

2.1. Synthesis of $La_2Ti_{1-x}V_xO_7$ nanocrystals

The $La_2Ti_{1-x}V_xO_7$ was synthesized using La_2O_3 (Yamanaka Hutech, 99.99 %) as lantallum, TiO_2 (Sigma Aldrich, 99 %) as titanium and Na_3VO_4 (Sigma Aldrich, 99.98 %) as vanadium sources. LiCl (Kanto, 99.95 %) was used as the molten salt. To synthesize the desired materials, 2 mol of La_2O_3 and 2 mol of TiO_2 were reacted with 1 mol of Na_3VO_4 in 2 mol of LiCl at 1000°C for 12 h. Using a muffle furnace, the ramping rate was set to 10°C min^{-1} and the cooling rate was set to 2°C min^{-1}. After cooling down, the products were washed with distilled water to obtain $La_2Ti_{1-x}V_xO_7$ powder. To compare with the $La_2Ti_{1-x}V_xO_7$ crystals structure, the $La_2Ti_2O_7$ was synthesized with the reaction of 1 mol of La_2O_3 and 2 mol of TiO_2 in 2 mol of LiCl at 800°C for 1 h. The ramping rate was set to 10°C min^{-1} and the cooling rate was set to 2°C min^{-1}. After cooling down, the products were washed with distilled water to obtain $La_2Ti_2O_7$ powder.

2.2. Structure characterization of $La_2Ti_{1-x}V_xO_7$ nanocrystals

$La_2Ti_{1-x}V_xO_7$ and $La_2Ti_2O_7$ powders were characterized using X-ray diffraction (XRD, Rigaku RINT Ultima with monochromated Cu-Kα radiation). Nanostructure analysis was carried out by scanning electron microscopy-energy dispersive X-ray (SEM-EDX, Hitachi, S-4800) and transmission electron microscopy (TEM, JEM-2100). The elemental analysis of samples was examined by X-ray photoelectron spectroscopy (XPS, ULVAC, Quantera SXM). Photoabsorption spectra of $La_2Ti_{1-x}V_xO_7$ and $La_2Ti_2O_7$ films were measured using a Hitachi U-4000 spectrophotometer.

2.3. Photoelectrochemical measurement of $La_2Ti_{1-x}V_xO_7$ nanocrystals electrode

$La_2Ti_{1-x}V_xO_7$ and $La_2Ti_2O_7$ paste electrodes were prepared using FTO films with a thickness of 0.5 μm. The electrodes were synthesized by a solution process using spin-coating of $La_2Ti_{1-x}V_xO_7$ and $La_2Ti_2O_7$ precursor prepared at room temperature [18]. It was followed by thermal annealing in air at 100°C for 30 mins. The photoelectrochemical measurements were performed with a three-electrode cell combining the $La_2Ti_{1-x}V_xO_7$ and $La_2Ti_2O_7$ electrodes with a saturated calomel reference electrode and a platinum counter electrode in the aqueous Na_2SO_4 electrolyte [16, 17]. The current-voltage characteristics were obtained using a potentiostat under intermittent UV light irradiation (Xe lamp with a light intensity of 100 mW/cm^2).

3. Results and Discussions

The XRD patterns of $La_2Ti_{1-x}V_xO_7$ powder synthesized using La_2O_3, TiO_2 and Na_3VO_4 with LiCl as molten salt at 1000ºC were shown in Fig. 1(a). The XRD patterns of $La_2Ti_{1-x}V_xO_7$ powder indicated that the crystal structure was monoclinic, comparable to $La_2Ti_2O_7$ powder according to the ICSD PDF number 1950. Since the primary crystal of $La_2Ti_{1-x}V_xO_7$ is $La_2Ti_2O_7$, the XRD pattern of $La_2Ti_{1-x}V_xO_7$ was compared with that of $La_2Ti_2O_7$. In a $La_2Ti_2O_7$ unit cell, titanium and oxygen atom are octahedrons. Moreover, each corner shares La^{3+} cations and no evident displacement happens for Ti^{4+} cations in TiO_6 oxygen octahedrons. The substitution of Ti^{4+} cations caused the V^{5+} cations to go inside the TiO_6 oxygen octahedron. The ionic radii of V^{5+} and Ti^{4+} were 0.54 Å and 0.605 Å, respectively. The substitution of Ti^{4+} cations by V^{5+} cations may distort TiO_6 oxygen octahedrons unit cell.

To observe the nanostructures of $La_2Ti_{1-x}V_xO_7$ and $La_2Ti_2O_7$ samples, SEM and TEM measurements were performed, as shown in Fig. 2. A plate-like structure of $La_2Ti_2O_7$ nanocrystals with a diameter of 500-600 nm was observed. By adding the vanadium ions, a cubic-shaped $La_2Ti_{1-x}V_xO_7$ was formed in a molten salt reaction. At a temperature higher than the melting point of LiCl (550 °C), the nucleation and crystal growth of $La_2Ti_{1-x}V_xO_7$ occurred in the molten salt reaction. The substituting of Ti^{4+} cations with V^{5+} cations inside the TiO_6 oxygen octahedron probably led to the expansion of crystal growth in this direction, producing the cubic shape morphology. As a molten salt, LiCl has successfully added vanadium ions in a unit cell structure of TiO_6 octahedron of $La_2Ti_2O_7$. The LiCl has likely assisted the synthesis by facilitating a homogeneous reaction from plate-like $La_2Ti_2O_7$ to cubic-shaped $La_2Ti_{1-x}V_xO_7$. The measurements of a single particle of $La_2Ti_{1-x}V_xO_7$ and $La_2Ti_2O_7$ samples nanocrystals were performed in Fig. 2. The

aggregated particles of $La_2Ti_{1-x}V_xO_7$ consisting of tiny nanocrystals were formed with a diameter of 300 nm.

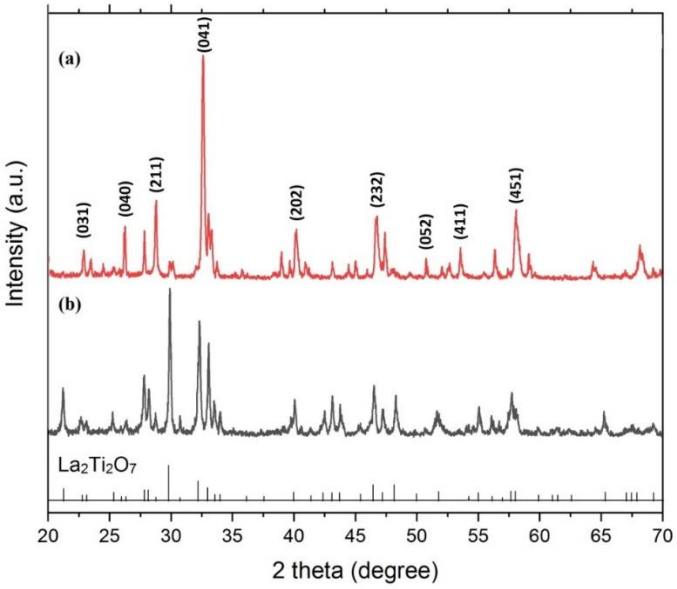

Fig. 1. XRD patterns of the (a) $La_2Ti_{1-x}V_xO_7$ and (b) $La_2Ti_2O_7$ samples synthesized using LiCl as molten salt.

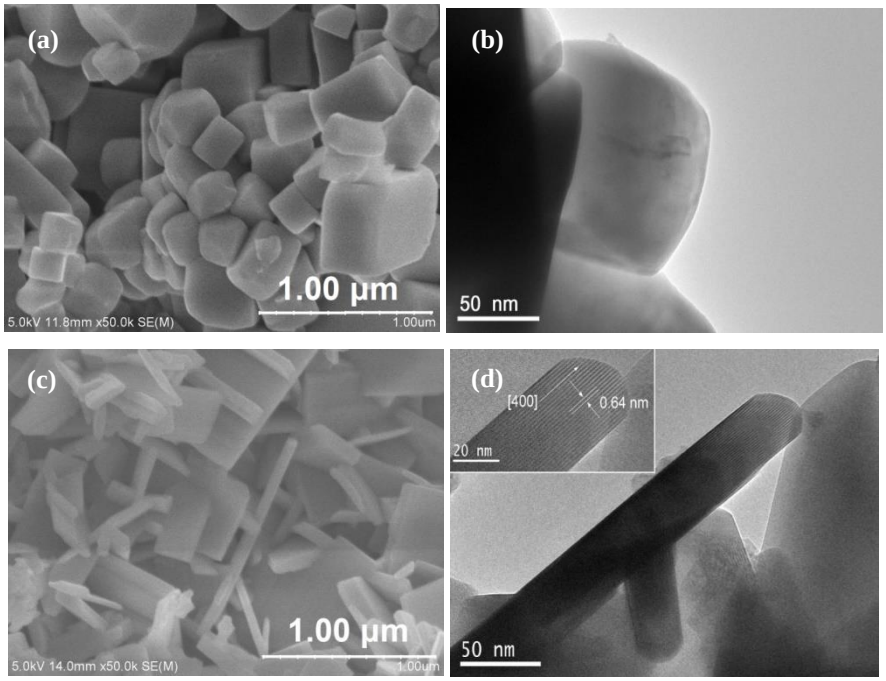

Fig. 2. The SEM and TEM images of the (a) and (b) $La_2Ti_{1-x}V_xO_7$ (c) and (d) $La_2Ti_2O_7$ samples.

The atomic compositions of the samples were analyzed by EDX, as shown in Table 1 and Fig. 3. In Table 1, the atomic concentration of La, Ti and O of $La_2Ti_2O_7$ sample was 19.42, 18.13 and 62.45%, respectively. The EDX analysis showed only La, Ti and O elements with the ratio La : Ti was 1.07, which is in the acceptable nominal composition of $La_2Ti_2O_7$ [13]. In contrast, the ratio of La : Ti in the $La_2Ti_{1-x}V_xO_7$ sample was 1.62. The increase of La : Ti ratio was caused by substituting of Ti^{4+} cations with V^{5+} cations inside the TiO_6 oxygen octahedron. At the same time, no impurities were observed, indicating that the dopant V^{5+} cation has been contained within the TiO_6 oxygen octahedrons and a solid $La_2Ti_{1-x}V_xO_7$ was formed.

Table 1. The compositions of $La_2Ti_{1-x}V_xO_7$ and $La_2Ti_2O_7$ samples.

	$La_2Ti_2O_7$ sample				$La_2Ti_{1-x}V_xO_7$ sample			
Compounds	**La**	**Ti**	**V**	**O**	**La**	**Ti**	**V**	**O**
Percentage	19.42	18.13	0	62.45	21.43	13.23	9.97	55.37

The XPS spectra of $La_2Ti_2O_7$ and $La_2Ti_{1-x}V_xO_7$ were presented in Fig. 3. In the $La_2Ti_2O_7$ sample, a photoelectron spectrum was attributed to the constituent element core level of La, Ti and O. C1s associated to hydrocarbons adsorbed on the surface were ascribed to the peak at 284.6 eV [19, 20]. The chemical bonding of $La_2Ti_2O_7$ should be characterized by the $La3d_{5/2}$, $La3d_{3/2}$, $Ti2p_{3/2}$ and O1s lines. When lanthanum and titanium interact with oxygen, valence electrons are transferred from metals to oxygens with variations in the inner shells' electrical screening.

The binding energy of $La3d_{5/2}$ was 851.8 eV and 855.8 eV, and the binding energy of $3d_{3/2}$ was 834.9 eV and 838.6 eV. The binding energies of $Ti3p_{3/2}$ and O1s were 458.1 eV and 529.8 eV, respectively. The binding energies of $La3d_{5/2}$, $La3d_{3/2}$, $Ti2p_{3/2}$ and O1s were consistent with the reported values for $La_2Ti_2O_7$ [19, 20]. In contrast, for the $La_2Ti_{1-x}V_xO_7$ sample spectrum, the shifting of binding energies of $La3d_{5/2}$, $La3d_{3/2}$, $Ti2p_{3/2}$ and O1s was observed indicating the binding composition change compared to $La_2Ti_2O_7$. The binding energy of $La3d_{5/2}$ and $La3d_{3/2}$ were 850.2 eV and 854.5 eV; 833.5 eV and 837.7 eV. The binding energies of $Ti2p_{3/2}$ and O1s were 457.1 eV and 528.7 eV, respectively. The V2p peak with the binding energy of 515 eV was observed in the $La_2Ti_{1-x}V_xO_7$ sample, indicating the presence of a chemical bond.

In order to determine the band gap energy of the materials, the absorption spectra of $La_2Ti_{1-x}V_xO_7$ and $La_2Ti_2O_7$ films were measured from 350 nm to 600 nm. The band gaps of $La_2Ti_{1-x}V_xO_7$ and $La_2Ti_2O_7$ samples were estimated to be 2.62 eV and 3.43 eV, respectively, as shown in Fig. 4. The value of band gap of $La_2Ti_2O_7$ synthesized using molten salt was consistent with the reported value for $La_2Ti_2O_7$ [21]. With the addition of the vanadium atoms, there are more atomic orbitals overlap. Consequently, the number of molecular orbitals increases and the band gap decreases from 3.43 eV to 2.62 eV.

As shown in Fig. 5, the photoresponse observed for all samples electrodes contained n-type semiconductors. Ordinarily, the onset potentials of anodic photocurrent of $La_2Ti_{1-x}V_xO_7$ electrode was -0.65 V vs. SCE. The highest anodic photocurrent was 18.41 μAcm^{-2} for $La_2Ti_{1-x}V_xO_7$ and 9.20 μAcm^{-2} for $La_2Ti_2O_7$ electrode at 1.0 V. To understand the carrier transport of sample electrodes, we have compared the donor density of the sample electrodes using Mott-Schottky

plots, as shown in Table 2. The donor density of the $La_2Ti_{1-x}V_xO_7$ sample electrode was 3.5 x 10^{15} cm^{-3}. This was higher than that of the $La_2Ti_2O_7$ sample electrode (7.2 x 10^{14} cm^{-3}). Vanadium dopant could effectively increase the carrier transport [22], leading to the higher photocurrent in the $La_2Ti_{1-x}V_xO_7$ electrode.

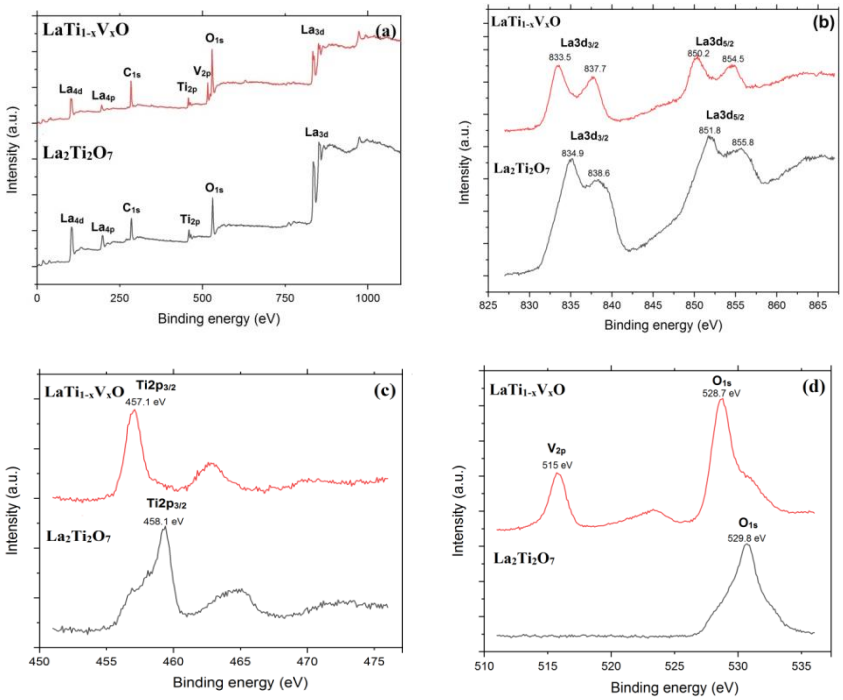

Fig. 3. The comparable photoelectron spectra of $La_2Ti_{1-x}V_xO_7$ and $La_2Ti_2O_7$ samples (a) whole region, (b) La3d, (c) Ti2p and (d) O1s and V2p.

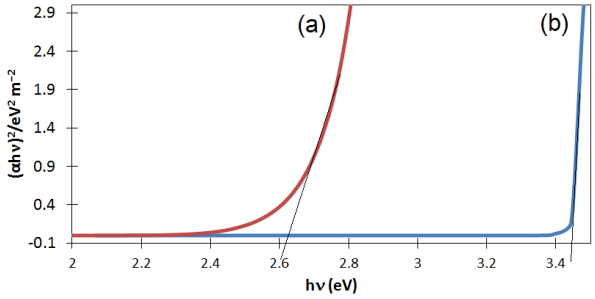

Fig. 4. The band gap estimations of (a) $La_2Ti_{1-x}V_xO_7$ and (b) $La_2Ti_2O_7$ films.

Table 2. The photoelectrochemical properties of $La_2Ti_{1-x}V_xO_7$ and $La_2Ti_2O_7$ electrodes.

Sample electrode	Onset potential V_{on} (V vs. SCE)	Photocurrent density at 1.0 V (μAcm^{-2})	Donor density (N_D) (10^{14} cm^{-3})
$La_2Ti_{1-x}V_xO_7$	-0.65	18.41	35
$La_2Ti_2O_7$	-0.43	9.20	7.2

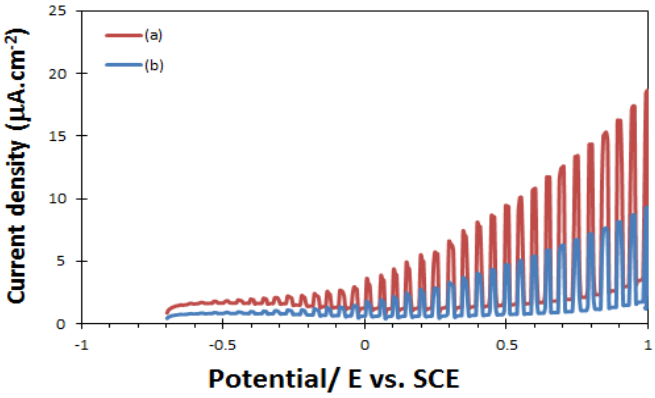

Fig. 5. Current-potential curves of the sample electrodes under intermittent UV irradiation. Sample were prepared using (a) $La_2Ti_{1-x}V_xO_7$ and (b) $La_2Ti_2O_7$ electrodes.

4. Conclusions

In summary, a cubic-shaped $La_2Ti_{1-x}V_xO_7$ has been successfully synthesized for the first time through the reaction of La_2O_3, TiO_2 and Na_3VO_4 using LiCl as the molten salt. The cubic-shape $La_2Ti_{1-x}V_xO_7$ nanocrystals were obtained by molten salt reaction at the temperature of 1000°C for 12 h. The XPS spectrum revealed that the substitution of Ti^{4+} cations by V^{5+} cations in $La_2Ti_{1-x}V_xO_7$ was not followed by the disruption of the unit cell. Notably, the photoelectrochemical cell fabricated using $La_2Ti_{1-x}V_xO_7$ nanocrystals showed a higher anodic photocurrent than the $La_2Ti_2O_7$ sample electrode. The photoelectrochemical property of the $La_2Ti_{1-x}V_xO_7$ nanocrystals electrode suggested the potential application for photocatalytic reaction.

References

1. Yan, H.; Ning, H.; Kan, Y.; Wang, P.; and Reece, M.J. (2009). Piezoelectric ceramics with super-high curie points. *Journal of American Ceramic Society*. 92, 2270.
2. Wang, Z.; Teramura, K.; Hosokawa, S.; and Tanaka, T. (2015). Photocatalytic conversion of CO_2 in water over Ag-modified $La_2Ti_2O_7$. *Applied Catalysis, B: Environmental*, 163, 241.
3. Kim, J.; Hwang, D.W.; Kim, H.-G.; Bae, S.W.; Ji, S.M.; and Lee, J.S. (2002). Nickel-loaded $La_2Ti_2O_7$ as a bifunctional photocatalyst. *Chemical Communications*, 2488.
4. Huang, Z.; Liu, J.; Huang, L.; Tian, L.; Sen Wang; Zhang, G.; Li, J.; Liang, F.; Zhang, H.; Jia, Q.; and Zhang, S. (2020). One-step synthesis of dandelion-like lanthanum titanate nanostructures for enhanced photocatalytic performance. *NPG Asia Mater*ials, 12.
5. Hwang, D.W.; Cha, K.Y.; Kim, J.; Kim, H.G.; Bae, S.W.; and Lee, J.S. (2003). Photocatalytic degradation of CH_3Cl over a nickel-loaded layered perovskite. *Industrial & Enginerring Chemistry Research*, 42, 1184.

6. Arney, D.; Porter, B.; Greve, B.; and Maggard, P.A. (2008). New molten-salt synthesis and photocatalytic properties of $La_2Ti_2O_7$ particles. *Journal of Photochemistry and Photobiology A: Chemistry*, 199, 230.
7. Abe, R.; Higashi, M.; Sayama, K.; Abe, Y.; and Sugihara, H. (2006). Photocatalytic activity of R_3MO_7 and $R_2Ti_2O_7$ (R= Y, Gd, La; M= Nb, Ta) for water splitting into H_2 and O_2. *The Journal of Physical Chemistry B*, 110 (5), 2219-2226.
8. Ma, Q.; Zhang, W.; and Young, J. (2022). Effect of single atom Platinum (Pt) doping and facet dependent on the electronic structure and light absorption of Lanthanum Titanium Oxide ($La_2Ti_2O_7$): A Density Functional Theory study. *Surface Science*, 715, 121949.
9. Erdem, M.; Cantürk, S.B.; and Eryürek, G. (2022). Upconversion Yb^{3+}/Er^{3+}: $La_2Ti_2O_7$ phosphors for solid-state lighting and optical thermometry. *Spectrochiica Acta-Part A: Molecular and Biomolecular Spectroscopy*. 270, 120854.
10. Hong, H.; McChesney, J.L.; Wrobel, F.; Yan, X.; Li, Y.; Bhattacharya, A.; and Fong, D.D. (2022). In situ study on the evolution of atomic and electronic structure of $LaTiO_3/SrTiO_3$ system. *Physical Review Materials.* 6, L011401.
11. Li, M.; Han, N.; Zhang, X.; Wang, S.; Jiang, M.; Bokhari, A.; Zhang, W.; Race, M.; Shen, Z.; Chen, R.; and Mubashir, M. (2022). Perovskite oxide for emerging photo(electro)catalysis in energy and environment. *Environmental Research.* 205, 112544
12. Hu, B.L.; Han, J.Y.; Ge, S.W.; Hua, X.J.; Li, S.L.; Xing, H.R.; Wang, K.S.; Hu, P.; Fu, J.B.; Zhang, W.; and Volinsky, A.A. (2022). Secondary phases strengthening-toughening effects in the Mo–TiC–La_2O_3 alloys. *Materials Science and Engineering: A.* 831, 142271.
13. Zhu, Y.; Xu, J.; and Chen, M. (2022). Synthesis of $La_2Ti_2O_7/Bi_5O_7I$ photocatalysts with improved photocatalytic activity for degradation of CIP under visible light. *Separation and Purification Technology*. 282, 120004.
14. Li, Y.; Xu, M.; Yan, X.; Addiego, C.; Jiang, L.; Wang, H.; and Zhu, J. (2021). Origin of the Enhanced Piezoelectricity of Vanadium-Doped $La_2Ti_2O_7$ Ceramics. *Journal of Physical Chemistry C*, 125(47), 26180-26187.
15. Li, Y.; Lee, T.; Jiang, L.; Wang, W.; Jiao, Z.; Liang, D.; Yan, X.; Xu, M.; Chen, Q.; Pan, X.; and Zhu, J. (2020). Improved Electrical Properties of Layer Structured $La_2Ti_{1.96}V_{0.04}O_7$ Ceramics. *Journal of Electronic Materials*, 49, 4, 2584-2595.
16. Purwiandono, G.; Manseki, K.; and Sugiura, T. (2020). Photo-electrochemical property of 2D hexagonal-shape GaN nanoplates synthesized using solid nitrogen source in molten salt. *Journal of Photochemistry and Photobiology A: Chemistry*, 394, 112499.
17. Purwiandono, G.; Manseki, K.; and Sugiura, T. (2020). A molten salt-based nitridation approach for synthesizing nanostructured InN electrode materials. *RSC Advances*, 10, 37576.
18. Vafaei, S.; Wolosz, A.; Ethridge, C.; Schnupf, U.; Hattori, N.; Sugiura, T.; and Manseki, K. (2021). Elucidation of the Crystal Growth Characteristics of SnO_2 Nanoaggregates Formed by Sequential Low-Temperature Sol-Gel Reaction and Freeze Drying. *Nanomaterials*, 11, 1738.

19. Atuchin, V.V.; Gavrilova, T.A.; Grivel, J.C.; and Kesler, V.G. (2008). Electronic structure of layered ferroelectric high-k titanate $La_2Ti_2O_7$. *Journal of Physics D: Applied Physics*, 42.
20. Lu, Y.; Le Paven, C.; Nguyen, H.V.; Benzerga, R.; Le Gendre, L.; Rioual, S.; Tessier, F.; Cheviré, F.; Sharaiha, A.; Delaveaud, C.; and Castel, X. (2013). Reactive sputtering deposition of perovskite oxide and oxynitride lanthanum titanium films: structural and dielectric characterization. *Crystal Growth & Design*, 13, 4852.
21. Bai, L.; Cai, Z.; and Xu, Q. (2021). A plasmonic photocatalyst of Ag@ AgBr/$La_2Ti_2O_7$ with enhanced photocatalytic activity under visible light irradiation. *Applied Physics A*, 127, 595.
22. Sun, S.; He, L.; Yang, M.; Cui, J.; and Liang, S. (2022). Facet Junction Engineering for Photocatalysis: A Comprehensive Review on Elementary Knowledge, Facet-Synergistic Mechanisms, Functional Modifications, and Future Perspectives. *Advanced Functional Materials*, 32, 2106982.